

Air-Sea Interaction

Harry Hendon
BMRC
GPO Box 1289k
Melbourne, 3001
Australia

hh@bom.gov.au

14 October, 2004

8.1 Introduction

Air-sea interaction associated with tropical intraseasonal variability and, particularly, the MJO is of interest for three reasons. First, variations of the air-sea fluxes of heat and moisture may be fundamental to mechanisms of tropical intraseasonal variability. For instance, air-sea interaction may promote the slow eastward propagation of the MJO and its northward propagation in the Indian summer monsoon. Besides playing a critical role for the interplay between convection and dynamics, surface fluxes of heat, moisture, and momentum drive SST perturbations that may feedback to the surface fluxes and ultimately to the atmospheric dynamics, thus, for instance, contributing to the growth of the MJO. Second, the episodic variations of surface momentum, heat and freshwater fluxes driven by atmospheric intraseasonal variability may play a role in the maintenance and low frequency variability of the warm pool in the tropical Indian and Pacific Oceans. For example, the MJO induces transports in the equatorial west Pacific that act in the mean to remove about the same amount of heat from the warm pool as is provided by the mean surface heat flux (Ralph et al. 1997). From the opposite perspective of the ocean driving the atmosphere, interannual variations of SST in the warm pool may also drive interannual variations in MJO activity, which may bear on the ability to predict seasonal variations of MJO activity. Finally, the MJO forces surface currents that drive SST variations at the eastern edge of the warm pool (e.g., Kessler et al. 1995). Kelvin waves are also efficiently excited by the MJO (e.g., Hendon et al. 1998), which radiate into the eastern Pacific where they can perturb the SST (e.g., Giese and Harrison 1991; Zhang 2001; McPhaden 2002). These intraseasonal SST variations may lead to a rectified coupled- response, which plays a role in the evolution of ENSO (e.g., Bergman et al. 2001; Zhang and Gottschalck 2002).

The focus in this chapter is on observations of air-sea interaction that may be relevant to the mechanism and variability of the MJO. The interactions relevant to the evolution of ENSO are only briefly discussed but are covered in detail in Chapters 7 and 10. Diagnostic studies of the

response in the upper ocean to intraseasonal surface flux variations, which provides insight into the processes that control the associated SST variability in the warm pool, are also covered.

Theory and modeling studies of the role of air-sea interaction for the mechanism for the MJO are touched upon briefly but are treated in detail in Chapters 2 and 11.

8.2 Air-sea fluxes for the eastward MJO

The evolution of surface heat, moisture and momentum fluxes associated with the eastward propagating MJO has been described in the western Pacific using satellite and in situ observations (e.g., Zhang 1996, Lau and Sui 1997, Zhang and McPhaden 2000) and across the entire warm pool using global analyses (e.g., Flatau et al. 1997; Hendon and Glick 1997, Jones et al. 1998, Shinoda et al. 1998, Woolnough et al. 2000). The basic structure of the fluxes is schematically illustrated in Figure 8.1 (from Shinoda et al. 1998). The abscissa (in kilometers) spans $\frac{1}{2}$ wavelength of the MJO, which is an equivalent duration of ~ 30 days at a given point as the MJO systematically propagates eastward. This schematic is typical for the MJO (with some minor shifts in phasing as discussed below) across the entire warm pool of the Indian and western Pacific oceans.

In the convectively active phase, which has a zonal extent of about 8000 km and meridional width of about 2000 km, increased deep convection is associated with increased cloud cover, increased rainfall, and decreased surface insolation. Enhanced deep convection slightly leads (~ 1 week) enhanced surface westerlies. In the warm pool region where the basic state wind is weak westerly, these anomalous westerlies act to increase the surface windspeed, hence increasing the flux of latent and sensible heat. In the convectively suppressed phase, which has a slightly larger zonal extent (and longer duration) than the active phase, reduced westerlies act to reduce the windspeed, thus reducing the latent and sensible heat flux. Decreased convection is also associated with decreased cloud cover and increased surface insolation.

The observed phase lag (~ 1 week) of latent heat flux with respect to enhanced convection is counter to that assumed in some simple “quasi-equilibrium” models of the MJO, whereby

enhanced latent heat flux to the east of enhanced convection acts to intensify convection to the east (e.g., Emanuel 1987). Such models presume an easterly basic state so that easterly anomalies in advance of enhanced convection act to increase the windspeed and latent heat flux. While such simple theory is at odds with the observed phase lag of latent heat flux with respect to convection, a positive impact of wind-induced latent heat flux variations has been demonstrated in some models (e.g., Neelin et al. 1987; Lin et al. 2000; Raymond 2001; Colón et al. 2002)

Magnitudes of the fluxes at the extrema of a large MJO event are indicated in Fig. 8.1. The sensible heat flux anomaly is not shown, as it is about 1/10 the size of the latent heat flux anomaly and has similar phasing. The net surface longwave radiation (also not shown) tends to oppose the surface insolation anomaly but is much smaller. Hence, the surface heat flux variation is dominated by the insolation and latent heat flux variations.

Enhanced convection and associated enhanced cloud cover typically reduce surface insolation by about $20\text{--}40\text{ Wm}^{-2}$. Shortly thereafter (~ 7 day lag), the latent heat flux, in association with enhanced surface westerlies, peaks with similar magnitude. This near collocation implies that the latent heat flux and insolation anomaly act together to produce a peak surface cooling of $40\text{--}80\text{ Wm}^{-2}$, which propagates coherently eastward across the equatorial warm pool in conjunction with the convection and surface westerly anomalies. In the suppressed convective phase, insolation is increased by $10\text{--}30\text{ Wm}^{-2}$ and the reduced surface westerlies act to decrease the latent heat flux by $10\text{--}30\text{ Wm}^{-2}$. Together the insolation and latent heat flux anomalies produce a peak surface warming of about $20\text{--}60\text{ Wm}^{-2}$ during the suppressed phase. Note that in this analysis, the peak amplitude of the warming during the suppressed convective phase is weaker than the cooling during the enhanced convective phase. However, the suppressed phase is of longer duration (greater zonal extent) than the enhanced phase. Hence, averaged over a life cycle the net heat flux is weakly positive into the warm pool.

As the convective anomaly approaches the dateline, induced easterly anomalies east of the convection act to increase the windspeed and latent heat flux (e.g., Hendon and Glick 1997;

Woolnough et al. 2000) because the mean (trade) winds are easterly in the eastern Pacific. Because enhanced latent heat flux now occurs east of enhanced convection (i.e., in a region of enhanced insolation) and the convective anomalies weaken as the MJO propagates into the eastern Pacific (hence producing weaker surface insolation anomalies), the surface heat flux perturbation is generally small east of the date line. However, during northern summer, the MJO perturbs convection in the ITCZ north of the equator and coherent surface heat flux perturbations of similar phasing and magnitude to those in the warm pool are observed in the eastern Pacific (e.g., Maloney and Kiehl 2002).

The MJO also perturbs the freshwater and surface momentum fluxes. Over the warm pool, Shinoda et al. (1998) estimate rainfall to increase by 5-7 mm d⁻¹ during the enhanced convective phase and decrease by a similar amount during the calm-suppressed convective phase. Similarly, westerly stress increases to about 0.05 Nm⁻² during the westerly-convective phase and decreases to about 0.01 Nm⁻² during the suppressed convective phase. A hallmark of the MJO is that the maximum (westerly) stress nearly coincides with the highest flux of freshwater into the ocean. Hence, their individual influences on the buoyancy forcing of the warm pool mixed layer will tend to cancel (e.g., Anderson et al. 1996; Zhang and Anderson 2003).

The phasing and relative magnitude of the fluxes in Fig. 8.1 are observed to vary systematically as the MJO traverses the Indian and western Pacific Oceans. When convection is developing in the Indian Ocean, the convective anomaly tends to be near the node of the surface zonal wind anomaly (e.g., Hendon and Salby 1994), which is consistent with a Gill-type response to equatorially-symmetric diabatic heating. As the convection moves into the western Pacific, the surface zonal wind anomaly shifts eastward relative to the convection so that anomalous westerlies blow entirely through the region of anomalous convection. Hendon and Salby (1994) interpreted this changing phase as indicative of the evolution of the energetics of the MJO through its lifecycle. However, a simple dynamical explanation is that the convective anomaly tends to be equatorially-centered in the Indian Ocean but shifts off the equator into the South

Pacific Convergence Zone in the west Pacific. Hence, the phasing of the surface zonal wind relative to convection in the Indian Ocean is consistent with an equatorial symmetric heat source. In the western Pacific, however, the phasing of the surface zonal winds is consistent with an equatorial asymmetric heat source displaced into the Southern Hemisphere.

The changing phase of the surface zonal winds relative to the convective anomaly implies that the phasing of the surface fluxes will change as the active convective phase propagates eastward from the Indian Ocean. In the western Pacific, the surface insolation anomaly will be more in phase with the latent heat flux anomaly because the surface westerlies coincide with increased convection. But, in the Indian Ocean, there will be less cooperation. Shinoda et al. (1998) further diagnosed the latent heat flux anomaly to contribute less to the total surface heat flux anomaly in the Indian Ocean. Hence, the surface heat flux variation in the Indian Ocean is dominated by the insolation variation whereas the latent heat and insolation anomalies make equal contributions in the western Pacific.

8.3 Air-sea fluxes associated with northward propagation in the Indian summer monsoon

During boreal summer, the eastward propagating MJO is notably weaker (e.g., Salby and Hendon 1994), while the dominant intraseasonal mode exhibits pronounced northward propagation ($\sim 1^\circ$ lat/day) from the equatorial Indian Ocean into the Indian monsoon (e.g., Sikka and Gadgil 1980; Wang and Rui 1990; Kemball-Cook and Wang 2001). The dominant period is shorter as well (35 days as compared to 50 days during winter). There is some debate as to whether northward propagation occurs independent of the eastward propagating MJO along the equator (e.g., Lawrence and Webster 2002; Jiang et al. 2004). Nonetheless, the northward propagating events during boreal summer significantly perturb the surface fluxes of heat, moisture and momentum. The associated coherent SST anomalies are indicative of robust air-sea (e.g., Bhat et al. 2001; Sengupta and Ravichandran 2001; Vecchi and Harrison 2002; Webster et al. 2002). While dynamical mechanisms for the poleward propagation away from the equator, which involve emitted Rossby waves, have been suggested (Chapter 2), air-sea interaction

appears to foster the northward propagation in much the same fashion as it fosters eastward propagation along the equator (e.g., Fu et al. 2003).

Figure 8.2 (from Kemball-Cook and Wang 2001) displays the structure of the air-sea fluxes for the typical northward propagating intraseasonal oscillation in the Indian Ocean sector during boreal summer. The abscissa spans about 20-25° latitude, representative of a section of the Indian Ocean from the equator to 20-25°N. Equivalently, a span of about 20 days is displayed at a given point in the Indian Ocean as the oscillation propagates by to the north.

To the north of the developing convective anomaly, reduced convection acts to increase the surface insolation. In the suppressed region, anomalous easterlies act on the westerly basic state of the summer monsoon, thereby reducing the windspeed and latent heat flux. During the convective phase, enhanced convection acts to decrease insolation, while anomalous westerlies act on the westerly basic state to increase the windspeed and latent heat flux. Typical magnitudes of these intraseasonal variations are $\sim 5 \text{ ms}^{-1}$ for the zonal wind, and $\sim 25 \text{ Wm}^{-2}$ for latent heat flux and insolation. These anomalies can increase by a factor of 3 to 4 for individual events (e.g., Webster et al. 2002).

As for the eastward propagating MJO, the maximum latent heat flux anomaly occurs slightly after the maximum convection, which again brings into question the relevance of simple “quasi-equilibrium” theories for explaining the intraseasonal behavior during boreal summer. The insolation anomaly slightly leads the latent heat flux anomaly, but they still add constructively to perturb the net surface heat flux, which can result in significant SST perturbations.

8.3 SST variability

For the ocean to play an active role in the dynamics of the eastward propagating MJO and the northward propagating variability in the Indian monsoon, the surface flux variations must induce a SST variation. Krishnamurti et al. (1988), motivated by the need to explain the long time scale of the MJO, were the first to examine SST variability associated with the MJO. Using data

from the FGGE year, they showed that intraseasonal (30-60 d period) SST variability was most prominent across the equatorial Indian and western Pacific Oceans and had temporal phasing indicative of the atmosphere forcing the ocean on the intraseasonal timescale (i.e., minimum SST lagged maximum surface westerlies by $\sim 1/4$ cycle). Hendon and Glick (1997), using seven years of weekly SST analyses from Reynolds and Smith (1994), confirmed their results. Figure 8.3 displays the ratio (as a percentage) of intraseasonal (30-90d period) to subseasonal (periods 10-200 d) SST variance. The regions in the Indian and western Pacific with ratio greater than 50% are also regions where SST variability exhibits a significant spectral peak near 60 days (Zhang 1996; Hendon and Glick 1997). These regions are also where the signal in convection and surface winds associated with the MJO is the strongest (e.g., Salby and Hendon 1994). Note that the intraseasonal variability in the northern Indian Ocean may be underestimated in the satellite-based SST data used to create Fig. 8.3 due to retrieval problems in regions of persistent precipitating convection (Harrison and Vecchi 2001; Sengupta and Ravichandran 2001).

For the eastward propagating MJO, warm SST anomalies develop after passage of the calm-suppressed phase, when the surface heat flux is most positive into the ocean, and cold SST anomalies develop after passage of the windy-convective phase, when the surface heat flux is most negative (Fig. 8.1). The typical SST anomaly has amplitude $\sim 1/3$ K (Flatau et al. 1997; Hendon and Glick 1997; Zhang 1997; Shinoda et al. 1998; Woolnough et al 2000; Kimball-Cook and Wang 2001), although strong MJO events often produce SST swings of more than 1 K in the western equatorial Pacific (e.g., Weller and Anderson 1996).

Pronounced SST anomalies in the Indian Ocean are also observed during boreal summer when the intraseasonal oscillation is propagating northward. To the north of the developing convective anomaly in the equatorial Indian Ocean, clear skies (enhanced insolation) and reduced latent heat flux (easterly anomalies) act to warm the Arabian Sea and Bay of Bengal (e.g., Kimball-Cook and Wang 2001; Vecchi and Harrison 2002). During the convective phase, increased cloud cover reduces insolation and anomalous westerlies act to increase the windspeed

and latent heat flux, thereby producing surface cooling. Hence, a warm SST anomaly leads the northward propagating convective anomaly by 1-2 weeks (1/4 cycle) and a cold SST anomaly follows the convective anomaly by a similar lag. The magnitude of these SST anomalies, especially in the Bay of Bengal (1-3 K), can be much larger than for the near-equatorial SST anomalies associated with the eastward propagating MJO (e.g., Sengupta and Ravichandran 2001). The freshness of the mixed layer in the Bay of Bengal, where mean precipitation and river runoff is high, results in a shallower and more stably stratified mixed layer with a deeper barrier layer than in the western equatorial Pacific (e.g. Bhat et al. 2001; Sengupta and Ravichandran 2001; Webster et al. 2002). Hence, the mixed layer in the Bay of Bengal remains shallow in the presence of stronger winds and is more sensitive to the intraseasonal surface heat flux variations.

8.4 Mechanisms of SST variability

Understanding how SST and the upper ocean mixed layer vary intraseasonally is important both for successful coupled simulation and for validation of air-sea interaction theories of intraseasonal variability. The focus in this section is on mechanisms of near-equatorial SST variability associated with the eastward MJO. Much less work has been done on the mechanisms of SST variability in the northern Indian ocean associated with northward propagating intraseasonal oscillations during boreal summer, probably due to lack of quality observations of the upper ocean and surface meteorology. However, recent field campaigns (e.g., JASMINE and BOBMEX) and new satellite SST products (e.g., Vecchi and Harrison 2002) have revealed some similarities and differences with the behavior of the near-equatorial warm pool, which are commented on at the end of this section.

The near-equatorial warm pool is a region of weak winds and horizontal SST gradient, deep thermocline (~100m), and shallow (~25 m), and fresh (stable) mixed layer, which overlays a deeper, more saline isothermal layer (e.g., Lukas and Lindstrom 1991). The layer between the halocline, which typically defines the base of the mixed layer, and the thermocline is referred to as the barrier layer, because it effectively shields the mixed layer from colder sub-thermocline

water. These conditions of weak horizontal temperature gradient and strong vertical stability mean that 1-dimensional processes primarily govern the intraseasonal SST variations in the warm pool. The relatively weak wind fluctuations produced by the MJO are typically not sufficient to mix through the barrier layer. Hence the SST variation associated with the MJO is primarily accounted for by surface heat flux variation (Anderson et al. 1996; Flatau et al. 1997; Hendon and Glick 1997; Lau and Sui 1997; Jones et al. 1998; Shinoda and Hendon 1998; Woolnough et al. 2000; Schiller and Godfrey 2002; Zhang and Anderson 2003). The largest heat flux out of the ocean occurs at about the time of maximum convection (Fig. 8.1), resulting in minimum SST about $\frac{1}{4}$ cycle later (about two weeks for the typical MJO event). Similarly, the largest heat flux into the ocean occurs at the time of most suppressed convection, resulting in warmest SST about $\frac{1}{4}$ cycle prior to onset of deep convection.

Detailed observations in the western equatorial Pacific during TOGA-COARE (Webster and Lukas 1992), however, suggest a complex evolution of the upper ocean through the life cycle of the MJO. TOGA-COARE ran from November 1992 through February 1993. The experiment was fortunate in that two major MJO events traversed the Intensive Flux Array (IFA) located in the equatorial western Pacific (roughly spanning 2N-2S, 152-157E) in December 1992 and January 1993 (e.g., Gutzler et al. 1994). Hourly observations of surface fluxes and SST at the IMET mooring (located at 1.45°S, 156°E; Weller and Anderson 1996) are shown in Fig. 8.4 (Anderson et al. 1996). During the suppressed convective phase, SST gradually warms in the presence of a positive surface heat flux and weak surface wind. A pronounced diurnal cycle of SST is evident. During the convective phase, when the winds strengthen and become westerly, the surface heat flux is negative and SST rapidly cools with an absence of a diurnal cycle. The westerlies at this time are seen to be highly variable, which is a hallmark of the so-called westerlies wind bursts that tend to occur within the large-scale envelope of enhanced convection during the MJO (e.g., Hendon and Liebmann 1994). These wind bursts could potentially play an

important role in the evolution of the warm pool mixed layer because the wind stirring of the mixed layer does not simply increase linearly with the windspeed.

High resolution modeling of the mixed layer indicates that 1-dimensional processes govern this SST behavior provided that accurate surface fluxes are utilized (Fig. 8.4; also Shinoda and Hendon 1998). However, for this TOGA-COARE period at the IMET site, a cumulative systematic bias is apparent (Fig. 8.4), which is only accounted for by considering horizontal and vertical advection (e.g., Cronin and McPhaden 1997, Feng et al. 1998, Feng et al. 2000). Except within the oceanic equatorial radius of deformation ($\sim 2\text{-}3^\circ$ latitude; e.g., Ralph et al. 1997; Feng et al. 2000; Shinoda and Hendon 2001; Schiller and Godfrey 2002), horizontal and vertical advection appear not to be coherent on the scale of the MJO. Hence, advection does not play a systematic role in governing the meridionally broad SST variation associated with the MJO (Shinoda and Hendon 1998, 2001). While advective processes are clearly important at some places for individual events, they depend critically on the initial state of the upper ocean (e.g., preexisting anomalous horizontal temperature gradient) and the atmospheric noise (the non-spatially coherent circulation). Thus, the magnitude and sign of the advective tendencies varies significantly from one MJO event to another. Systematic advection in the near equatorial belt is returned to shortly.

The mixed layer depth does vary systematically over the life cycle of the MJO (Hendon and Glick 1997; Shinoda and Hendon 1998), which will affect the sensitivity of the mixed layer to surface heat flux variations and the amount of shortwave radiation that penetrates through the mixed layer. Mixed layer deepening is also indicative of entrainment, which may act to additionally cool or warm the mixed layer depending on the stratification.

The typical evolution of the ocean mixed layer from the suppressed-calm phase to the convective-windy phase of the MJO is illustrated in Fig. 8.5 (from Shinoda and Hendon 1998). During the calm-clear phase of the MJO (day 36-48), which corresponds to 26 November- 8 December 1992 during COARE, a shallow mixed layer forms above a deep barrier layer in

response to positive surface heat flux and small turbulent mixing. A strong diurnal cycle of mixed layer depth and temperature develops (Fig. 8.6), with nighttime convection acting to spread the intense daytime warming to a deeper layer. The shallowness of the mixed layer during this warming phase (<10 m) also results in significant ($>10 \text{ Wm}^{-2}$) penetration of shortwave radiation through the base of the mixed layer. Absorption of this radiation below the mixed layer results in a stable inversion owing to the freshness of the mixed layer (Lukas and Lindstrom 1991; Sprintall and Tomczak 1992; Anderson et al. 1996; Shinoda and Hendon 1998; Schiller and Godfrey 2002; Zhang and Anderson 2003).

During the cloudy-windy phase (days 68 –70, which corresponds to 26-28 December 1992), the surface heat flux is negative, the mixed layer deepens and the diurnal cycle of radiation is weak. The negative surface heat flux initially cools the mixed layer more than the sub mixed-layer and the mixed layer begins to deepen, eroding the barrier layer. Entrainment of submixed layer water into the mixed layer initially acts to warm the mixed layer because of the slight (but stable) temperature inversion in the barrier layer. Thus, the entrainment heat flux into the mixed layer tends to be out of phase with the surface heat flux (Shinoda and Hendon 1998); diurnal entrainment (nighttime convection) during the surface warming phase cools the mixed layer, while entrainment of warm sub-mixed layer water during the surface cooling phase tends to warm the mixed layer.

In the experiments of Shinoda and Hendon (1998) cold sub-thermocline water was never entrained into the mixed layer during the windy-convective phase because of the weakness of the large-scale MJO-induced winds, the strong stratification at the thermocline in the initial conditions, and the development of a barrier layer during the calm-clear phase. However, entrainment of sub-thermocline water into the mixed layer is observed to occur in the western Pacific during some strong westerly wind bursts (e.g., Feng et al. 1998). The results of Shinoda and Hendon (1998) suggest that over the large spatial scale of the typical MJO, entrainment

cooling during the cloudy-windy phase of the MJO is not systematic but may be important during some intense events.

The phasing of the mixed layer depth (deepest during the cloudy-windy phase and shallowest during the calm-clear phase) does result in enhanced sensitivity of the mixed layer temperature to surface heat flux forcing during the warming phase and reduced sensitivity during the cooling phase. The enhanced sensitivity during the warming phase is partially offset by an increased amount of shortwave radiation that penetrates through the base of the shallow mixed layer. Still, if the mean mixed depth is used to simulate the MJO-induced SST variation, then the cooling phase is over predicted and the warming phase is under-predicted by 25-50% (Shinoda and Hendon 1998).

Lukas and Lindstrom (1991) and Anderson et al. (1996) suggest that the intraseasonal variation of freshwater flux may also play a role in governing the mixed layer evolution over the course of the MJO. They envision that intense precipitation prior to the windy-cooling phase would generate a very stable fresh mixed layer, hence preventing mixing of cold water into the mixed layer during the windy-cooling phase. While such behavior has been observed at individual locations throughout the warm pool (e.g., Sprintall and Tomczak 1992), the phasing of the freshwater flux relative to the surface cooling and maximum surface windspeed for the MJO (Fig. 8.1) suggests that it is not an important process for the typical MJO event. That is, the bulk of the rainfall during the MJO tends to fall during the windiest period, thus preventing formation of a shallow fresh layer (e.g., Zhang and Anderson 2003).

Shinoda and Hendon (1998) showed the lack of sensitivity to the freshwater flux variation associated with the MJO by driving the mixed layer model with composite surface fluxes from 10 well-defined MJO events. Two simulations were conducted. The control run used the full surface fluxes for each MJO event, while the other run prescribed the freshwater flux to be held constant at its mean value. Very little difference in mixed layer temperature is predicted. Hence, while the mean freshwater flux is critical for maintaining the freshness and stratification

of the warm pool (e.g., Lukas and Lindstrom 1991; Anderson et al. 1996), the intraseasonal variation of freshwater flux over the life cycle of the MJO appears not to be systematically important. Zhang and Anderson (2003) point out that accurate simulation in climate models of the phasing of rainfall and winds for the MJO is challenging. Hence, coupled models may erroneously simulate sensitivity to the freshwater flux simply by simulating an MJO with an unrealistic phasing of rainfall relative to the windspeed maximum.

Inclusion of the diurnal cycle of insolation, on the other hand, does have a large systematic impact on the evolution of the mixed layer temperature. Figure 8.7 (from Shinoda and Hendon 1998) shows the daily mean mixed layer temperature predicted at the IMET mooring during TOGA COARE for simulations using hourly surface fluxes and daily mean surface fluxes. During the calm-clear phases of the MJO, when the diurnal cycle of mixed layer temperature is large, inclusion of the diurnal cycle of insolation increases the daily mean mixed layer temperature by 0.2-0.5 K. More heat is absorbed in a shallower mixed layer during daylight hours when the insolation and mixed layer depth vary diurnally, even though nighttime convection tends to spread this heat out over a deeper layer. Hence, the mean SST during the calm phase increases. The amplitude of the intraseasonal variation of SST over the life cycle of the MJO also increases by 20-30% (see also Schiller and Godfrey 2002). Impact of this amplified intraseasonal SST variation on the atmosphere and specifically on the dynamics of the MJO has yet to be determined. On the other hand, the diurnal cycle of SST during the suppressed phase has been postulated to drive shallow convection in the afternoon that acts to progressively moisten the lower troposphere, setting up conditions that are favorable for the onset of organized convection within the MJO (Godfrey et al. 1998).

The broad-scale surface wind perturbations associated with the MJO, though typically weak ($<5 \text{ ms}^{-1}$), do act to rapidly spin up a near-equatorial surface current (e.g., McPhaden et al. 1988; Maes et al. 1998; Cronin et al. 2000; Shinoda and Hendon 2001). These currents may then advect both the mean zonal SST gradient on the eastern edge of the warm pool (which may be

relevant to the initiation of El Niño and as discussed in Chapters 7 and 10) and the anomalous zonal SST gradient in the warm pool induced by the MJO via the surface heat flux variations (Ralph et al. 1997). An example of such a narrow equatorial jet (i.e., Yoshida 1959) was observed with drifters during TOGA COARE (Ralph et al. 1997). This strong eastward current developed in response to the surface westerlies associated with the MJO event that traversed the western Pacific in late December 1992. The narrow, meridionally convergent jet is well simulated by an ocean general circulation model forced with observed surface stress for this period (Fig. 8.8 from Shinoda and Hendon 2001).

Ralph et al. (1997) demonstrate that this jet acted to advect eastward the anomalous cold SST that developed in the equatorial western Pacific in response to the MJO-induced surface cooling. They further diagnosed that, in the long term mean, such nonlinear advection acts to cool the equatorial western Pacific warm pool at just the rate that it is warmed by the net surface heat flux ($\sim 10 \text{ W m}^{-2}$). Hence, episodic nonlinear advection generated by the MJO helps to maintain the mean state of the warm pool. Shinoda and Hendon (2001) qualitatively confirmed this result by driving an ocean general circulation model with observed intraseasonal surface fluxes. But, the simulated mean cooling produced by the MJO was underestimated presumably due to difficulties in predicting subtle changes to the weak zonal SST gradient.

Much less work has been done on the mechanisms of SST variability in the northern Indian Ocean associated with northward propagating intraseasonal activity during boreal summer. Analysis of limited observations in the Bay of Bengal reveal a near-quadrature relationship between net surface heat flux variations associated with intraseasonal oscillations in convection and SST, consistent with the notion that the SST variation is primarily driven by the surface heat flux variation (Sengupta and Ravichandran 2001). Taking into account the variation of mixed layer depth and penetration of short wave radiation, Sengupta and Ravichandran (2001) showed qualitative agreement between the surface heat flux variation and observed intraseasonal SST tendency. Despite the fact that mean winds are strong ($\sim 10 \text{ ms}^{-1}$), abundance of rainfall and runoff

in the region maintains a stable mixed layer upon a deep barrier layer, which prevents mixing of cold subthermocline water into the mixed layer (Bhat et al. 2001). On the other, model results from Loschnigg and Webster (2000) suggest the oceanic poleward heat transport integrated across the entire Indian Ocean varies in association with the poleward propagating intraseasonal events. Their result implies that the intraseasonal oscillation drives changes in the wind-driven circulation of the Indian Ocean, but it is not clear how or whether these changes in heat transport relate to the associated SST changes.

8.5 SST-atmosphere feedback

One consequence of the induced intraseasonal SST variations is that the surface fluxes will be modified. The induced SST anomaly associated with the MJO (Fig. 8.1) has been diagnosed to cause a slight eastward shift of the latent heat flux anomaly relative to the windspeed anomaly because of the temperature effect on the surface saturation humidity (e.g., Zhang 1996; Hendon and Glick 1997). This eastward shift causes the maximum latent heat flux to be more collocated with the maximum convection, rather than lagging it by a few days. This subtle phase difference has important ramifications for the mechanism of the eastward propagating MJO (e.g., Raymond 2001). However, the quality of current global surface flux and humidity data sets prohibits a more definitive description at this time.

The induced SST anomaly will also act to reduce the sensible and latent heat fluxes driven by the MJO (Hendon and Glick 1997; Shinoda et al. 1998). That is, SST will warm in response to reduced latent heat flux in the suppressed phase, but a warmer SST will act to increase the latent heat flux. The opposite happens in the suppressed phase. Shinoda et al. (1998) estimate that the induced SST anomaly acts to reduce the amplitude of the latent heat flux by 10-15%. How this reduction may affect the dynamics of the MJO is not obvious, but in some atmospheric models coupled to shallow slab mixed layers (so that a large SST anomaly is induced) the MJO amplitude is diminished because the wind-evaporation feedback is effectively eliminated (E. Maloney, personal communication 2004).

The phasing of the SST anomalies relative to the convective anomaly, where by warm SST precedes enhanced convection by ~1-2 weeks and cold SST proceeds suppressed convection by a similar lag, is also suggestive of a positive feedback. Various mechanisms for a positive feedback of the SST perturbations onto the eastward propagating MJO have been proposed. Wang and Xie (1998), Waliser et al. (1999), Kemball-Cook et al. (2002), and Maloney and Kiehl (2002) propose that the warm SST in advance of the convective anomaly hydrostatically acts to lower the surface pressure, thereby promoting more moisture convergence in advance of the convective phase, thus helping to destabilize the MJO. This thermodynamically driven enhancement is estimated to directly account for about a 10% reduction in surface pressure and a similar increase in surface convergence. However, due to feedbacks between moisture convergence, diabatic heating and circulation, the total effect of this slight pressure reduction could be much larger. In the Waliser et al. and Kemball-Cook et al. studies, the SST-induced surface convergence acts to amplify a preexisting MJO mode in the models. On the other hand, in the Wang and Xie study, the SST-induced convergence acts to destabilize the MJO-mode for conditions where the model otherwise does not support an MJO.

Flatau et al. (1997), Hendon and Glick (1997), and Lau and Sui (1997) propose that the warm SST anomaly directly destabilizes the atmospheric column in advance of the convection by acting to raise the surface equivalent potential temperature (or moist static energy). At 30° C, a 0.5°C swing in SST is associated with a 0.8 g kg⁻¹ change in saturation mixing ratio or about a 3°C change in saturation equivalent potential temperature. In the Flatau et al. (1997) model, where the SST tendency was simply parameterized to be negative (cool) when the surface winds were westerly (which encompasses enhanced windspeed and reduced insolation due to enhanced convection) and positive (warm) when the surface winds were easterly (which encompasses reduced windspeed and enhanced insolation due to reduced convection), coupling with the SST acted to amplify, slow down, and better organize an existing MJO-like mode.

Judging the realism of these coupled model studies is difficult. In the Flatau et al. (1997) study, the induced SST anomalies are 3-4 times bigger than observed. Though coupling did dramatically improve the intraseasonal organization of convection and its eastward propagation, the impact of the induced SST anomalies may be over estimated. Waliser et al. (1999), using a slab-mixed layer coupled to a general circulation model, and Kemball-Cook et al. (2002), using an intermediate ocean model coupled to a general circulation, report more positive impacts whereby coupling slowed down and strengthened an existing MJO-like mode. While more realistic intraseasonal SST anomalies were simulated (amplitudes ~ 0.1 K), it is difficult to assess the robustness of these results based on short (10-15 year) integrations due to large internal variability of the MJO in the absence of coupling. However, coupling is certainly not a panacea for simulation of the MJO. Hendon (2000) found little impact of coupling in a general circulation model that produces a robust MJO-like mode when uncoupled. The uncoupled mode in this particular model appears to be promoted by evaporation-wind feedback (Neelin et al. 1987), with enhanced evaporation unrealistically occurring in the easterlies to the east of the convective anomaly. As a result, the latent heat flux and insolation anomalies do not constructively add to perturb the net surface heat flux, thus little SST anomaly is generated when coupled. The conclusion from these general circulation model studies, then, is that the coupling at best improves the simulation of the MJO, but only if it is reasonably simulated in the uncoupled models.

The near quadrature relationship between northward propagating convection during boreal summer and SST suggests that the ocean is primarily being forced by the atmosphere, similar to the situation for the eastward propagating MJO. But, as for the eastward MJO events, the warm SST anomaly in advance of the poleward propagating convective anomaly acts to hydrostatically decrease surface pressure, thereby increasing surface convergence and humidity, which acts to destabilize the atmosphere in advance of the convection (e.g., Kemball-Cook et al 2002; Fu et al. 2003). While northward propagation of the MJO is simulated in some models to

occur in the absence of air-sea coupling, inclusion of coupling increases the amplitude of the northward propagating events by ~50% (Fu et al. 2003). In fact, the impact of air-sea coupling on northward propagation in the Indian summer monsoon appears to be more robust than that on eastward propagation of the MJO along the equator.

8.6 Impact of slow SST variations on MJO activity

Interaction of the MJO with the ocean has been discussed from the perspective of the atmosphere driving the ocean with the possibility of a coupled feedback. One way interaction, where by the slowly varying SST influences the behavior of the MJO, does play an important role for the seasonal and interannual variation of MJO activity. The seasonal variation of MJO activity, with the strongest eastward propagation occurring near vernal equinox (e.g., Salby and Hendon 1994), is partially explained by the seasonal cycle of SST and mean convection (e.g., Li and Wang 1994; Salby et al. 1994). The most zonally extensive warm pool and region of active convection develop after the austral solstice, but is displaced into the Southern Hemisphere. The strongest MJO activity tends to occur at this time because near-equatorial convection can develop in the Indian Ocean and propagate furthest east into the Pacific. At the autumnal equinox, intraseasonal convection is observed to peak again in the Indian Ocean (Salby and Hendon 1994), but because SSTs have not yet warmed in the equatorial western Pacific, MJO activity tends to not be as strong as near the vernal equinox.

Large year to year variability in the strength of MJO activity is also observed (e.g., Salby and Hendon 1994; Hendon 1999; Slingo et al. 1999). This variability, at least at that time of year when the MJO is strongest as measured by globally integrated indices, is not clearly connected to interannual variations of the SST. For instance Hendon et al. (1999) and Slingo et al. (1999) found little relationship between year to year variations of the level of global MJO activity and SST variations, and, in particular, those associated with ENSO. A possible exception is an apparent tendency for global MJO activity to weaken at the peak of the strongest El Nino events. Figure 8.9a, which is an updated version of the plot shown in Hendon et al. (1999), confirms the

lack of a simple relationship between MJO activity in austral summer (the season when MJO activity is strongest) and ENSO. This result has been confirmed with GCM studies where observed SST is prescribed for a number of years (e.g., Slingo et al. 1999; Gualdi et al. 1999; Waliser et al. 2001). However, simulation of the MJO in these models is far from perfect. Thus, there is ample scope for further study of seasonal predictability of the MJO once reliable simulations of the MJO are achieved.

On the other hand, a significant relationship between global MJO activity in boreal summer and ENSO is apparent (Fig. 8.9b). Despite the fact that this occurs at the time of year when the MJO is weakest along the equator, it is during this time of the year when MJO activity may have its greatest impact on the evolution of the coupled system in the Pacific (e.g., Fedorov 2002). A simple explanation for the enhanced MJO activity in boreal summer during developing El Niño events is that the total SST field then is similar to the normal SST field during late boreal winter. In particular, the cold tongue in the central and eastern Pacific, which normally acts to reduce eastward propagation along the equator during boreal summer (e.g., Li and Wang 1994) is absent during a warm event. Thus, MJO activity can propagate further east and maintain its strength longer. The lack of a relationship between the strength of global MJO activity and ENSO during boreal winter results because, as warm events peak in boreal winter, anomalous convection then often shifts so far east in the Pacific that suppressed conditions develop in the western Pacific. Thus, the MJO experiences less of a fetch upon which to grow.

MJO activity, along with all other intraseasonally varying convective activity, does shift eastward in the Pacific during warm events and contracts westward during cold events (Gutzler 1991; Anyamba and Weare 1995; Fink and Speth 1997, Hendon et al. 1999, Kessler 2001). This eastward shift appears to simply reflect the eastward shift of warm SST as El Niño develops: warming SST provides the basis for MJO activity to develop further eastward. Kessler (2001) points out that this apparently diagnostic relationship may still be supportive of an active role of the MJO in the development of El Niño, especially if the MJO produces a rectified response in

the western Pacific (e.g., Shinoda and Hendon 2002), where the coupled system is especially sensitive (e.g., Kessler and Kleeman 2000; and see Chapters 7 and 10).

8.7 Concluding remarks

This review has focused on observations of air-sea interaction associated with eastward and northward propagation of the MJO. Specifically, air-sea interactions that are relevant to the mechanism and variability of the MJO were addressed. Two areas of future research will shed more light onto the role of air-sea interaction for intraseasonal variability throughout the global tropics. First, improved global data sets from new observing platforms and refined reanalysis of surface fluxes, SST and rainfall will allow more comprehensive study of the delicate interplay of convection, SST and oceanic and atmospheric circulation. Second, improved simulation of tropical intraseasonal variability in climate models will allow careful study of the mechanism and importance of active coupling on intraseasonal time-scales.

8.8 Acknowledgement

While this chapter is purportedly a comprehensive review of tropical intraseasonal air-sea interaction, the perspective is a personal one. I thank S. Anderson, S. Kemball-Cook, and the American Meteorological Society for allowing me to reproduce Figs. 8.2 and 8.4. Comments on an earlier version of this chapter by C. Zhang and the editors lead to improvements in the presentation and scope.

8.9 References

- Anderson, S. P., R. A. Weller, and R. Lukas, 1996: Surface buoyancy forcing and the mixed layer in the western Pacific warm pool: Observation and 1D model results. *J. Climate*, **9**, 3056–3085.
- Anyamba, E. K., and B. C. Weare, 1995: Temporal variability of the 40–50 day oscillation in tropical convection. *Int. J. Climatol.*, **15**, 379–402.
- Bergman, J. W., H. H. Hendon, and K. M. Weickmann, 2001: Intraseasonal variation of west Pacific convection at the onset of the 1997–98 El Niño. *J. Climate.*, **14**, 1702–1719.
- Bhat, G.S., and co-authors, 2001: BOBMEX: The Bay of Bengal Monsoon Experiment. *Bull. Amer. Meteor. Soc.*, **82**, 2217–2243.
- Colón, E., J. Lindesay, and M.J. Suarez, 2002: The impact of surface flux-and circulation-driven feedbacks on simulated Madden-Julian Oscillations. *J. Climate*, **15**, 624–641.
- Cronin, M.F., M.J. McPhaden, and R.H. Weisberg, 2000, Wind–forced reversing jets in the western equatorial Pacific. *J. Phys. Ocean.*, **30**, 657–676.
- Cronin, M. F., and M. J. McPhaden, 1997: The upper ocean heat balance in the western equatorial Pacific warm pool during September–December 1992. *J. Geophys. Res.*, **102**, 8533–8553.
- Emanuel, K.A., 1987: An air-sea interaction model of intraseasonal oscillations in the Tropics. *J. Atmos. Sci.*, **44**, 2324–2340.
- Fedorov, A. V., 2002: The response of the coupled tropical ocean–atmosphere to westerly wind bursts. *Quart. J. Roy. Meteor. Soc.*, **128**, 1–23.
- Feng, M., P. Hacker, and R. Lukas, 1998: Upper ocean heat and salt balances in response to a westerly wind burst in the western equatorial Pacific during TOGA COARE. *J. Geophys. Res.*, **103**, 10289–10311.
- Feng, M., R. Lukas, P. Hacker, R. A. Weller, and S. P. Anderson, 2000: Upper-ocean heat and salt balances in the western equatorial Pacific in response to the intraseasonal oscillation during TOGA COARE. *J. Climate.*, **13**, 2409–2427.
- Fink, A., and P. Speth, 1997: Some potential forcing mechanisms of the year-to-year variability of the tropical convection and its intraseasonal (25–70 day) variability. *Int. J. Climatol.*, **17**, 1513–1534.
- Flatau, M., P.J. Flatau, P. Phoebus, and P.P. Niiler, 1997: The feedback between equatorial convection and local radiative and evaporative processes: the implications for intraseasonal oscillations. *J. Atmos. Sci.*, **54**, 2373–2386.
- Fu, X., B. Wang, T. Li, and J.P. McCreary, 2003: Coupling between northward propagating intraseasonal oscillations and sea surface temperature in the Indian Ocean. *J. Atmos. Sci.*, **60**, 1733–1753.

- Giese, B. S., and D. E. Harison, 1991: Eastern equatorial Pacific response to three composite westerly wind types. *J. Geophys. Res.*, **96**, (Suppl.),. 3239–3248.
- Godfrey, J.S., R.A. Houze, R.H. Johnson, R.Lukas, J.L. Redelsperger, A. Sumi, and R. Weller, 1998: Coupled Ocean-Atmosphere Response Experiment (COARE): An interim report. *J. Geophys. Res.*, **103C**, 14395-14450.
- Gualdi, S., A. Navarra, and G. Tinarelli, 1999: The interannual variability of the Madden–Julian oscillation in an ensemble of GCM simulations. *Climate Dyn.*, **15**, 643–658.
- Gutzler, D. S., 1991: Interannual fluctuations of intraseasonal variance of near-equatorial zonal winds. *J. Geophys. Res.*, **96**, 3173–3185.
- Gutzler, D. S., G. N. Kiladis, G. A. Meehl, K. M. Weickmann, and M. Wheeler, 1994: The global climate of December 1992–February 1993. Part II: Large-scale variability across the tropical western Pacific during TOGA COARE. *J. Climate.*, **7**, 1606–1622.
- Harrison, D. E., and G. A. Vecchi, 2001: January 1999 Indian Ocean cooling event. *Geophys. Res. Lett.*, **28**, 317–3720.
- Hendon, H. H., 2000: Impact of air–sea coupling on the Madden–Julian oscillation in a general circulation model. *J. Atmos. Sci.*, **57**, 3939–3952.
- Hendon, H. H., C. Zhang, and J. D. Glick, 1999: Interannual variability of the Madden–Julian oscillation during austral summer. *J. Climate.*, **12**, 2538–2550.
- Hendon, H. H., B. Leibmann, and J. Glick, 1998: Oceanic Kelvin waves and Madden–Julian oscillation. *J. Atmos. Sci.*, **55**, 88–101.
- Hendon, H. H., and J. Glick, 1997: Intraseasonal air–sea interaction in the tropical Indian and Pacific Oceans. *J. Climate.*, **10**, 647–661.
- Hendon, H. H. and B. Liebmann, 1994: Organization of convection within the Madden Julian Oscillation . *J. Geophys. Res.*, **99**, 8073-8083.
- Hendon, H.H., M.L. Salby, 1994: The life cycle of the Madden–Julian Oscillation. *J. Atmos. Sci.*, **51**, 2225–2237.
- Jiang, X., T.Li, and B. Wang, 2004: Structures and mechanisms of the northward propagating boreal summer intraseasonal oscillation. *J. Climate*, **17**, 1022-1039.
- Jones, C., D. E. Waliser, and C. Gautier, 1998: The influence of the Madden–Julian oscillation on ocean surface heat fluxes and sea surface temperature. *J. Climate.*, **11**, 1057–1072.
- Kemball-Cook, S., B.Wang, and X. Fu, 2002: Simulation of the intraseasonal oscillation in ECHAM-4 model: The impact of coupling with an ocean model. *J. Atmos. Sci.*, **59**, 1433-1453.
- Kemball-Cook, S., and B. Wang, 2001: Equatorial waves and air–sea interaction in the boreal summer intraseasonal oscillation. *J. Climate*, **14**, 2923–2942.

- Kessler, W.S., 2001: EOF representations of the Madden–Julian Oscillation and its connection with ENSO. *J. Climate*, **14**, 3055–3061.
- Kessler, W. S., and R. Kleeman, 2000: Rectification of the Madden–Julian oscillation into the ENSO cycle. *J. Climate.*, **13**, 3560–3575.
- Kessler, W. S., M. J. McPhaden, and K. M. Weickmann, 1995: Forcing of intraseasonal Kelvin waves in the equatorial Pacific. *J. Geophys. Res.*, **100**, 10613–10631.
- Krishnamurti, T. N., D. K. Oosterhof, and A. V. Metha, 1988: Air–sea interaction on the timescale of 30–50 days. *J. Atmos. Sci.*, **45**, 1304–1322.
- Lau, K. M., and C.-H. Sui, 1997: Mechanisms of short-term sea surface temperature regulation: Observations from TOGA COARE. *J. Climate.*, **10**, 465–472.
- Lawrence, D.M., and P.J. Webster, 2002: The boreal summer intraseasonal oscillation: relationship between northward and eastward movement of convection. *J. Atmos. Sci*, **59**, 1593-1606.
- Li, T., and B. Wang, 1994: The influence of sea surface temperature on the tropical intraseasonal oscillation: A numerical study. *Mon. Wea. Rev.*, **122**, 2349–2362.
- Lin, J. W.-B., J.D. Neelin, and N. Zeng, Ning. 2000: Maintenance of tropical intraseasonal variability: impact of evaporation–wind feedback and midlatitude storms. *J. Atmos. Sci.*, **57**, 2793-2823.
- Loschnigg, J., and P.J. Webster, 2000: A coupled-atmosphere system of SST modulation for the Indian Ocean. *J. Climate*, **13**, 3342-3360.
- Lukas, R., and E. Lindstrom, 1991: The mixed layer of the western equatorial Pacific ocean. *J. Geophys. Res.*, **96**, (Suppl.), 3343–3357.
- Maes, C., P. Delecluse, and G. Madec, 1998: Impact of westerly wind bursts on the warm pool of the TOGA–COARE domain in an OGCM. *Climate Dyn.*, **14**, 55–70.
- Maloney, E. D., and J.T. Kiehl, 2002: MJO-related SST variations over the tropical Eastern Pacific during Northern Hemisphere summer. *J. Climate*, **15**, 675–689.
- McPhaden, M. J., 2002: Mixed layer temperature balance on intraseasonal timescales in the equatorial Pacific Ocean. *J. Climate*, **15**, 2632–2647.
- McPhaden, M.,J., H.P. Fretiag, S.P. Hayes, B.A. Taft, Z. Chen, and K.Wyrtki, 1988: The response of the equatorial Pacific Ocean to a westerly wind burst in May 1986. *J. Geophys., Res.*, **93**, 10 589-10 603.
- Neelin, J.D., I.M. Held, and K.H. Cook, 1987: Evaporation-wind feedback and low-frequency variability in the tropical atmosphere. *J. Atmos. Sci.*, **44**, 2341-2348.
- Ralph, E. A., K. Bi, and P. P. Niiler, 1997: A Lagrangian description of the western equatorial Pacific response to the wind burst of December 1992. *J. Climate.*, **10**, 1706–1721.

- Raymond, D. J., 2001: A new model of the Madden–Julian Oscillation. *J. Atmos. Sci.*, **58**, 2807–2819.
- Reynolds, R. W., and T. M. Smith, 1994: Improved global sea surface temperature analyses using optimum interpolation. *J. Climate.*, **7**, 929–948.
- Salby, M. L., and H. H. Hendon, 1994: Intraseasonal behavior of clouds, temperature, and winds in the Tropics. *J. Atmos. Sci.*, **51**, 2207–2224.
- Salby, M. L., G. Rolando , and H.H. Hendon, 1994: Planetary-scale circulations in the presence of climatological and wave-induced heating. *J. Atmos. Sci.*, **51**, 2344–2367.
- Sengupta, D., and M. Ravichandran, 2001: Oscillations of Bay of Bengal sea surface temperature during the 1998 summer monsoon. *Geophys. Res. Letter*, **28**, 2033–2036.
- Schiller, A., and J.S. Godfrey, 2003: Indian Ocean intraseasonal variability in an ocean general circulation model. *J. Climate*, **16**, 21–39.
- Shinoda, T., and H. H. Hendon, 2002: Rectified wind forcing and latent heat flux produced by the Madden-Julian Oscillation *J. Climate.*, **15**, 3500–3508.
- Shinoda, T., and H. H. Hendon, 2001: Upper-ocean heat budget in response to the Madden–Julian oscillation in the western equatorial Pacific. *J. Climate.*, **14**, 4147–4165.
- Shinoda, T., and H. H. Hendon, 1998: Mixed layer modeling of intraseasonal variability in the tropical western Pacific and Indian Oceans. *J. Climate.*, **11**, 2668–2685
- Shinoda, T., H. H. Hendon, and J. Glick, 1998: Intraseasonal variability of surface fluxes and sea surface temperature in the tropical western Pacific and Indian Oceans. *J. Climate.*, **11**, 1685–1702.
- Sikka, D.R., and S.Gadgil, 1980: On the maximum cloud zone and the ITCZ over Indian longitudes during the southwest monsoon. *Mon. Wea. Rev.*, **108**, 1840–1853.
- Slingo, J. M., D. P. Rowell, K. R. Sperber, and F. Nortley, 1999: On the predictability of the interannual behaviour of the Madden–Julian oscillation and its relationship to El Niño. *Quart. J. Roy. Meteor. Soc.*, **125**, 583–609.
- Sprintall, J., and M. Tomczak, 1992: Evidence of the barrier layer in the surface layer of the tropics. *J. Geophys. Res.*, **97**, 7305–7316.
- Vecchi, G.A., and D.E. Harrison, 2002: Monsoon breaks and subseasonal sea surface temperature variability in the Bay of Bengal. *J. Climate*, **15**, 1485–1493.
- Waliser, D E., Z. Zhang, K.M. Lau, and J.-H. Kim, 2001: Interannual sea surface temperature variability and the predictability of tropical intraseasonal variability. *J. Atmos. Sci.*, **58**, 2596–2615.
- Waliser, D. E., K.-M. Lau, and J. H. Kim, 1999: The influence of coupled sea surface temperatures on the Madden–Julian oscillation: A model perturbation experiment. *J. Atmos. Sci.*, **56**, 333–358.

- Wang, B., and H. Rui, 1990: Synoptic climatology of transient tropical intraseasonal convection anomalies: 1975–1985. *Meteor. Atmos. Phys.*, **44**, 43–61.
- Wang, B., and X. Xie, 1998: Coupled modes of the warm pool climate system. Part I: The role of air–sea interaction in maintaining Madden–Julian oscillation. *J. Climate*, **11**, 2116–2135.
- Webster, P. J., and co-authors, 2002: The JASMINE pilot study. *Bull. Amer. Meteor. Soc.*, **83**, 1603–1630.
- Webster, P. J., and R. Lukas, 1992: TOGA COARE: The Coupled Ocean–Atmosphere Response Experiment. *Bull. Amer. Meteor. Soc.*, **73**, 1377–1416.
- Weller, R. A., and S. P. Anderson, 1996: Surface meteorology and air–sea fluxes in the western equatorial Pacific warm pool during the TOGA coupled ocean–atmosphere response experiment. *J. Climate.*, **9**, 1959–1990.
- Woolnough, S. J., J. M. Slingo, and B. J. Hoskins, 2000: The relationship between convection and sea surface temperature on intraseasonal timescales. *J. Climate.*, **13**, 2086–2104
- Yoshida, K., 1959: A theory of the Cromwell current and of the equatorial upwelling—An interpretation in a similarity to a coastal circulation. *J. Oceanogr. Soc. Japan.*, **15**, 159–170.
- Zhang, C., 2001: Intraseasonal perturbations in sea surface temperatures of the equatorial eastern Pacific and their association with the Madden–Julian oscillation. *J. Climate.*, **14**, 1309–1322.
- Zhang, C., 1997: Intraseasonal variability of the upper-ocean thermal structure observed at 0° and 165°E. *J. Climate*, **10**, 3077–3092.
- Zhang, C., 1996: Atmospheric intraseasonal variability at the surface in the tropical western Pacific Ocean. *J. Atmos. Sci.*, **53**, 739–758.
- Zhang, C., and S.P. Anderson, 2003: Sensitivity of intraseasonal perturbations in SST to the structure of the MJO. *J. Atmos. Sci.*, **60**, 2196–2207.
- Zhang, C., and J. Gottschalck, 2002: SST anomalies of ENSO and the Madden–Julian Oscillation in the equatorial Pacific. *J. Climate*, **15**, 2429–2445
- Zhang, C., and M.J. McPhaden, 2000: Intraseasonal surface cooling in the equatorial western Pacific. *J. Climate*, **13**, 2261–2276

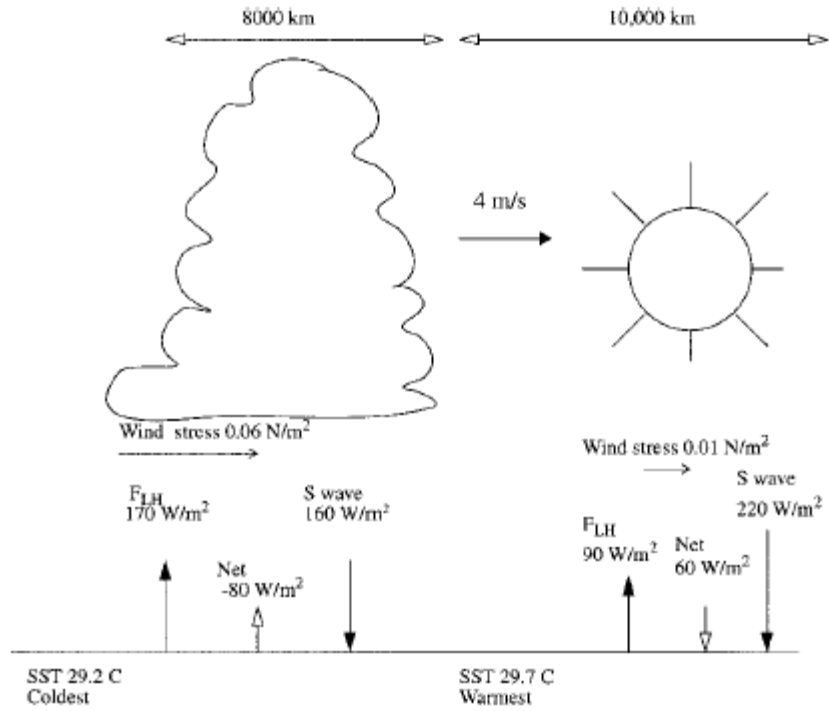


FIG. 8.1. Schematic diagram showing magnitude and phase relationship relative to the convective anomaly of the surface fluxes and SST variations produced by the canonical MJO. The asymmetric zonal scale of the cloudy-windy and suppressed-calm phases and eastward phase speed (4 m s^{-1}) of the joint atmosphere-ocean disturbance across the warm pool are indicated. Typical extrema of surface fluxes and SST over life cycle of MJO are shown for western Pacific. From Shinoda et al. (1998)

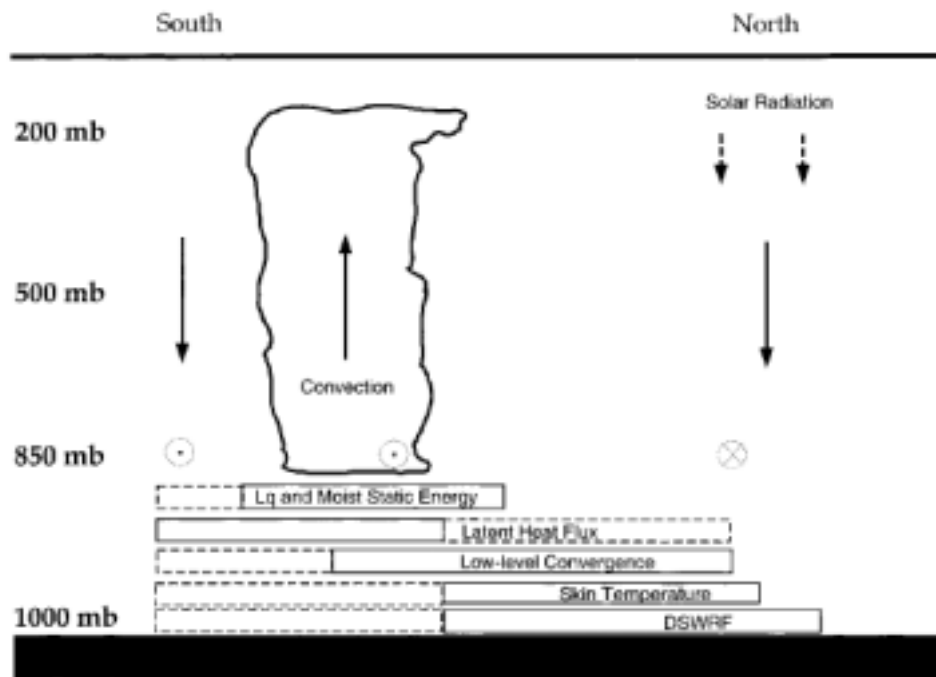


Fig. 8.2. Schematic of air–sea interaction in the northward propagation of convective anomalies associated with the intraseasonal oscillation during boreal summer in the Indian and western Pacific Oceans. Dark vertical lines indicate the mid-troposphere vertical velocity anomaly. The cloud indicates deep precipitating convection. The boxes represent the approximate locations of anomalies relative to the convection. Solid box indicates a positive anomaly, and dashed box indicates a negative anomaly. Circles indicate direction of 850-mb zonal wind anomaly with the \odot (\otimes) representing easterlies (westerlies). From Kemball-Cook and Wang (2001).

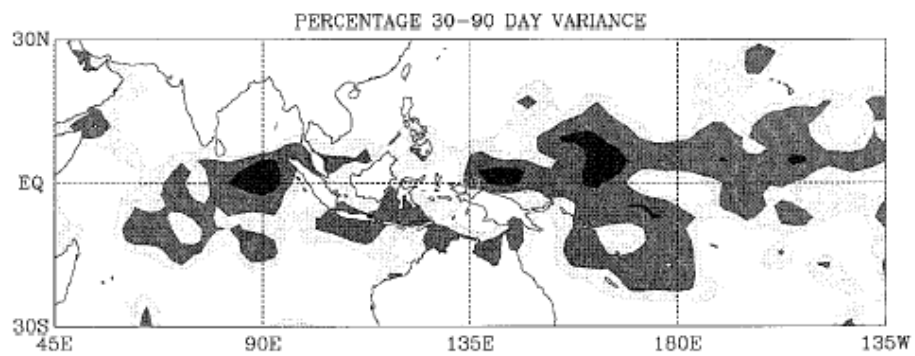


FIG. 8.2. Ratio (percentage) of intraseasonal (30–90-d period) SST variance to the total subseasonal (periods 10–200 d) SST variance for the period 1 July 1986–30 June 1993. Shading levels begin at 45%, 50%, and 60%. From Hendon and Glick (1997).

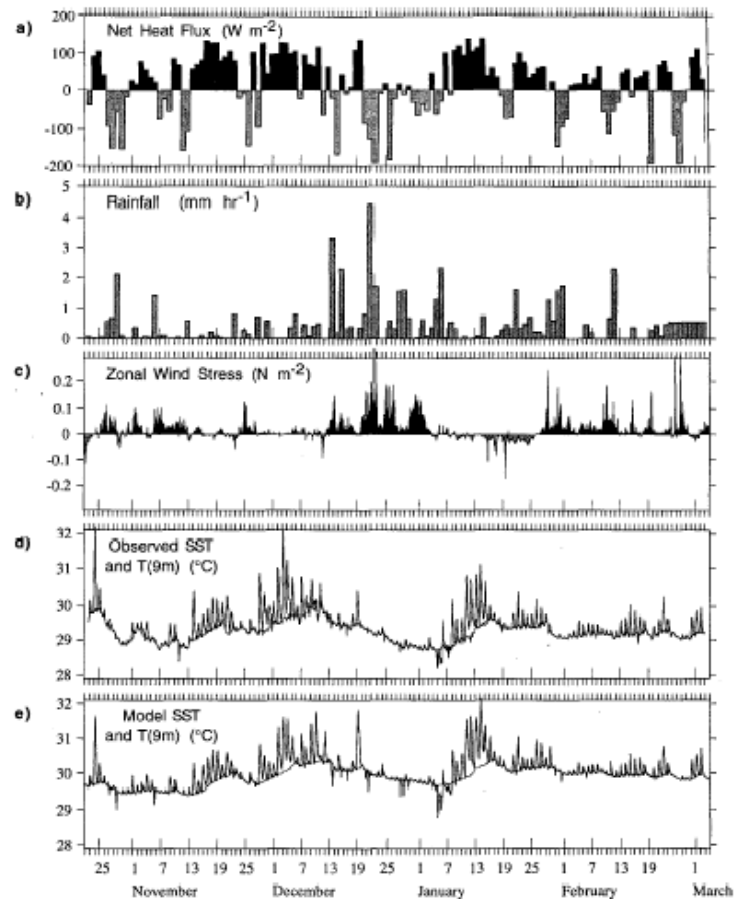


Fig. 8.3 Time series of air-sea fluxes and SST from WHOI IMET mooring located in IFA during TOGA COARE (25 October 1992-1 March 1993). The net heat flux and rainfall were averaged over 24 hours. The wind stress and observed SST were smoothed over 2 hours. The modeled SST was estimated using a 1-dimensional mixed layer model forced with the observed surface fluxes from the IMET mooring. From Anderson and Weller (1996).

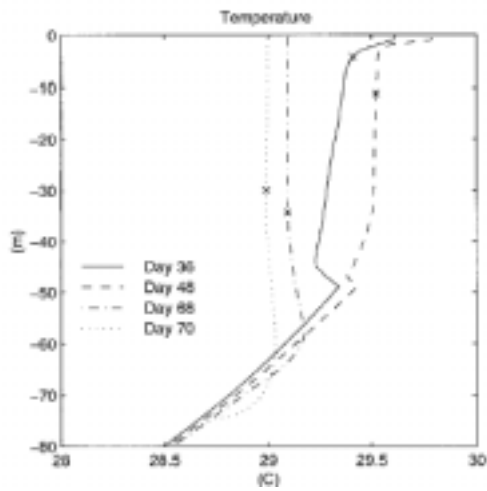


Fig. 8.4 Daily averages temperature profile simulated in the equatorial western Pacific with a 1-dimensional mixed layer model driven with observed surface fluxes for the MJO event that traversed the IFA in late December 1992 (see Fig. 5). The crosses indicate the mixed layer depth each day. Day 36 corresponds to 26 November 1992 (suppressed convective phase) and day 70 corresponds to 30 December 1992 (post convective phase). From Shinoda and Hendon (1998).

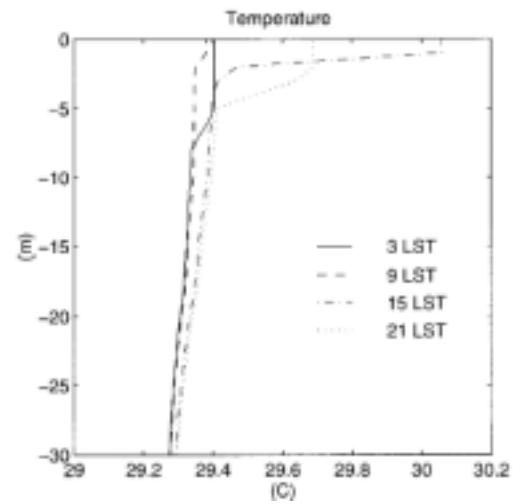


Fig. 8.5 Diurnal cycle of vertical temperature profile simulated during the suppressed convective phase of the MJO in the equatorial western Pacific on 26 November 1992. From Shinoda and Hendon (1998).

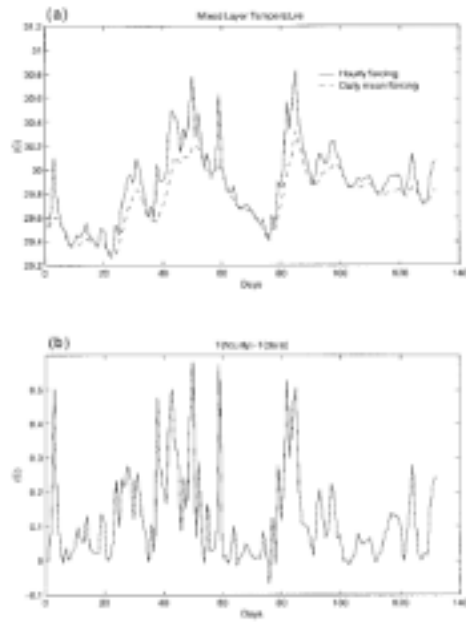


FIG. 8.6. Predicted SST at the IMET site for 22 October 1992–2 March 1993 using hourly surface fluxes from the IMET mooring data (thick curve) and daily mean fluxes (dashed curve). (b) The SST difference between the two experiments shown in (a). From Shinoda and Hendon (1998).

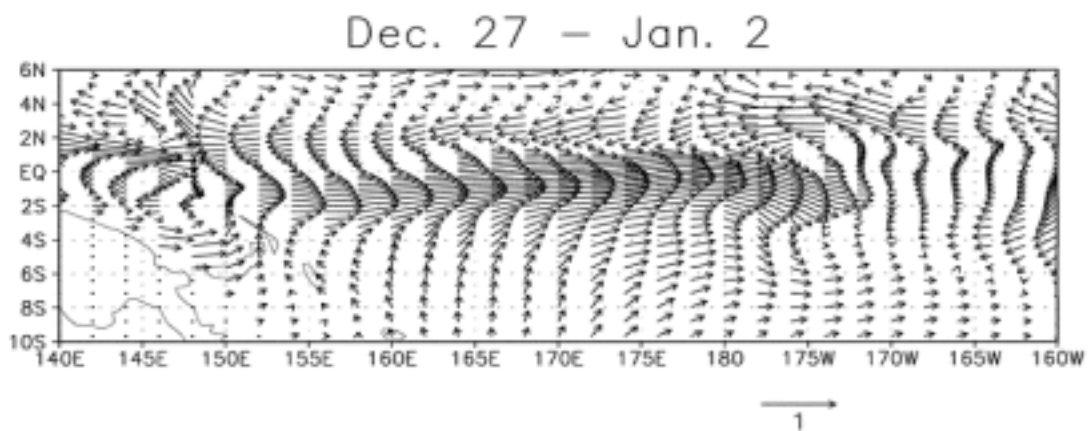


Fig. 8.7 Surface currents simulated for the week beginning 27 December 1992 using an ocean general circulation model driven with observed surface fluxes. The maximum velocity vector has magnitude 1 m s^{-1} . From Shinoda and Hendon (2001).

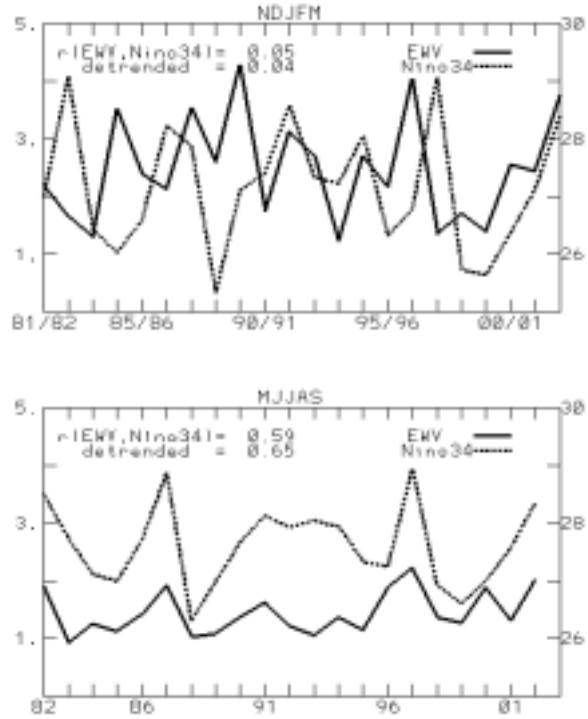


Fig 8.8 Time series of tropically averaged (15S-15N) OLR variance filtered to eastward wavenumbers 1-4 and periods 30-90 days. Top panel is for the five month period November through March and bottom panel is for May through September. Also shown is the Nino34 SST index for the same 5 month periods. Simultaneous correlations, with and without linear trend, are indicated. Filtered OLR data were kindly supplied by M. Wheeler, BMRC.